Journal of Biomedical Optics 6(2), 205–213 (April 2001)

Thermal effects in laser-assisted pre-embryo zona drilling

Diarmaid H. Douglas-Hamilton
Hamilton Thorne Research
102c Cummings Center
Beverly, Massachusetts 01915

Jérôme Conia
Cell Robotics Inc.
2715 Broadbent Parkway NE
Albuquerque, New Mexico 87107

Abstract. Diode lasers [$\lambda = 1480$ nm] are used with *in vitro* fertilization to dissect the zona pellucida (shell) of pre-embryos. A focused laser beam is applied *in vitro* to form a channel or trench in the zona pellucida. The procedure is used to facilitate biopsy or as a promoter of embryo hatching. We present examples and measurements of zona pellucida ablation using animal models. In using the laser it is vital not to damage pre-embryo cells, e.g., by overheating. In order to define safe regimes we have derived some thermal side effects of zona pellucida removal. The temperature profile in the beam and vicinity is predicted as function of laser pulse duration and power. In a crossed-beam experiment a HeNe laser probe is used to detect the temperature-induced change in the refractive index of an aqueous solution, and estimate local thermal gradient. We find that the diode laser beam produces superheated water approaching 200°C on the beam axis. Thermal histories during and following the laser pulse are given for regions in the neighborhood of the beam. We conclude that an optimum regime exists with pulse duration $\leqslant 5$ ms and laser power ~ 100 mW.
[DOI: 10.1117/1.1353796]

Keywords: embryo; laser; temperature; zona pellucida; infrared; microscope.

Paper 20019 received May 23, 2000; revised manuscript received Nov. 21, 2000; accepted for publication Nov. 21, 2000.

1 Introduction

A growing number of patients treated for infertility are undergoing *in vitro* fertilization (IVF) with assisted reproduction technologies. Some apparently healthy pre-embryos are impaired in their ability to hatch from their protective shell, the zona pellucida (ZP), after *in vitro* fertilization. Fortunately, it is possible to initiate hatching of the pre-embryos in the laboratory, before reimplantation in the reproductive tract of a patient.[1,2] In the laboratory, assistance is provided to these pre-embryos by creating a notch or channel—a region of stress release—in the zona for the purpose of improving the chances of successful implantation. After transfer into the uterus the embryo hatches: it extrudes itself through the channel and implants into the uterine wall. The ZP may be prepared using a focused beam of infrared (IR) light, and laser-assisted hatching can result in improving implantation and pregnancy success rates.[3] In addition, preimplantation genetic testing may also improve the success rate of IVF procedures. A panel of tests has been reported that can identify chromosomal abnormalities in the developing embryo before implantation, thus reducing the rate of spontaneous miscarriage.[4] Here again, IR lasers may be usefully applied to facilitate biopsy and the collection of important genetic clues from the pre-embryo in the laboratory.[5,6]

Precise channeling of the zona pellucida may be accomplished efficiently under microscopy using the ablative properties of pulsed laser radiation. A laser beam is introduced in the optical path of an inverted microscope and then tightly focused on the target zona pellucida using the same objective lens utilized to view the specimen. Since the pre-embryos are fragile and valuable, the procedure must be well controlled and very reliable. The wavelength of light, the duration of the pulse, the laser spot size, and the light energy delivered are all factors that must be taken into consideration when evaluating the safety of the procedure. Ultraviolet wavelengths are avoided since the potential for mutagenic effects exists. In contrast, these concerns are minimized with a near-infrared laser source. A laser operating at wavelength $\lambda = 1480$ nm is preferred because water molecules absorb strongly at this wavelength [attenuation coefficient $\alpha = 21\ \mathrm{cm}^{-1}$ (Ref. 7)], and destruction of tissue bonds is due mainly to heat transfer from water. Microscopic dissection of the zona pellucida at 1480 nm was first reported for animal models, in particular with specimens of murine origin. The well-established mouse model is advantageous because it is informative and the outcome of laser treatment can be readily studied after culturing the pre-embryos *in vitro* for only a few days.

In experiments using a 1480 nm diode laser with a range of laser pulse duration and intensity,[8,9] channels from 5 to 20 μm in diameter were drilled in the 7.5-μm-thick zona pellucida of mouse pre-embryos. The reported laser pulse duration τ was in the range $3 < \tau < 100$ ms, and laser power P in the range $22 < P < 70$ mW. Laser spot size was 2–8 μm and laser energy was 0.5–1.3 mJ. The safety of the procedure was evaluated by the absence of visible damage at the ultrastructural and biological levels.[9,10] No laser-induced structural alterations of the neighboring cytoplasm were observed after scan-

Address all correspondence to Diarmaid H. Douglas-Hamilton. Tel: 978-921-2050; Fax: 978-921-0250; E-mail: dhdh@hamiltonthorne.com

1083-3668/2001/$15.00 © 2001 SPIE

ning and transmission electron microscopy. Improved implantation rate was also observed after transfer of the treated pre-embryos in surrogate mothers.[3] After birth, the development of the mice was followed and no morphological anomaly was detected; the reproductive capacity of the mice was confirmed among subsequent generations.

Laser-mediated zona ablation with the 1480 nm diode laser was further applied to human pre-embryos. Laser-assisted hatching in pre-embryos recently resulted in successful clinical pregnancies and healthy babies.[11] In particular, assisted hatching of frozen–thawed pre-embryos with the 1480 nm laser enhanced pregnancy outcome in patients who had several previous implantation failures.[12] Opening of the zona pellucida and removal of degenerated pre-embryonic cells of frozen–thawed pre-embryos also increased implantation and pregnancy rates.[13]

As more successful pregnancy results are published, interest in laser applications with pre-embryos is likely to grow among both clinics and patients. However, as with any clinical application, the introduction of a new technology inevitably raises questions and/or fears of unexpected consequences. In particular, with all its promises of improvements, the application of laser technology to human pre-embryos must be prevented from being unintentionally harmful, for example, by overheating the blastomeres adjacent to the site of laser delivery. In previous experiments, measurements of laser heating in beams focused in medium with heat-sensitive molecules introduced into cells were made at $\lambda = 1064$ (used for optical tweezers), by Liu et al.[14] At 100 mW incident power, with $\lambda = 1064$ nm ($\alpha = 0.1\ \mathrm{cm}^{-1}$), they obtained steady state temperature rise near the focus of $\Delta T = 1.15°\mathrm{C}$. Recently Cellier and Conia[15] made interferometric longitudinal phase-change measurements, using 100 mW at $\lambda = 985$ nm ($\alpha = 0.42$), and obtained $\Delta T = 7.3°\mathrm{C}$. We can estimate the temperature rise that would have been obtained in these experiments at $\lambda = 1480$ nm. Since in a thermal-diffusion controlled situation the temperature will scale as αP, at $\lambda = 1480$ the above temperature increases would scale to $\Delta T \sim 242$ and 366°C, respectively. Such high values will cause significant local heating. A laser instrument for use in clinical practice must therefore be designed with extensive safety considerations in mind. In this paper, we present the evaluation of some thermal side effects of zona pellucida removal by laser as a function of various laser parameters. Limits to local heating are estimated. The temperature profile in the focused laser beam and in the nearby region as function of time is used to minimize potentially dangerous regimes of pulse duration and laser intensity.

2 Preliminary Experiments

2.1 Laser Module, Microscope Specifications and Design

We used a Nikon TE-300 laser-equipped inverted microscope, which has the IR laser beneath the stage. Laser light proceeds up through the objective and is focused on the target. The laser module (ZLTS, Hamilton Thorne Research, Beverly, MA) has maximum power 200 mW at $\lambda = 1480$ nm, and is utilized in pulsed mode. Peak transmitted laser power through the objective is ~140 mW. Pulse duration is adjustable in half millisecond increments from 0.5 to 25 ms. In addition to the laser diode itself, the laser module includes control board, adjustable collimating lens and dichroic mirror, and is interlocked to prevent potentially hazardous operation.

The laser module fits into the microscope filter cube slot under the stage, and the beam is deflected by a dichroic mirror along the optic axis of the microscope. The nearly collimated beam is directed toward the back aperture of a 40×, 0.60 numerical aperature (NA) objective lens, designed to maximize transmission at 1480 nm. The long working distance (WD = 3 mm) objective lens is used to focus the laser beam on to the target specimen; it has high transmission ratio in the infrared range (typically ~71% at 1480 nm). The collimation of the beam is adjusted to give parfocality of IR and visible light. Biological specimens, e.g., bovine oocytes or mouse pre-embryos, are maintained in an aqueous culture medium in clear polystyrene Petrie culture dishes (Falcon, Lincoln Park, NJ). The incident focused laser beam travels sequentially through air, plastic, and then the aqueous solution before reaching the target area of the zona pellucida.

Delivered laser energy at the objective was measured using a thermal detector head (Ophir Optronics, Peabody, MA) placed immediately above the stage with objective removed. Transmission of the objective was determined by placing an identical opposed objective above the focal point to recollimate the beam, which passed into the detector. Using the derived transmission, 71% at $\lambda = 1480$ nm, maximum beam power at the focal point was estimated at 103 mW, allowing for reflection at the polystyrene Petrie dish and absorption through 75 μm H_2O. Pulse duration was checked using an oscilloscope (Tektronix TDS 360) monitoring laser radiation scattered on to a Ge photodiode detector (B1918-01, Hammamatsu, Bridgewater, NJ). In a preliminary measurement, the focal beam radius in air was determined by intercepting the beam at the focal point with a knife edge, which was moved across the beam at known rate while the IR intensity was monitored with the Ge detector. At the focus, the radius to the $1/e^2$ intensity level was $R = 3.1 \pm 0.5\ \mu$m. The focal cone half angle in the medium is 26.7°.

2.2 Examples: Laser-Assisted Zona Dissection with Bovine Eggs

Bovine eggs are readily available. They constitute a useful and cost effective model for testing laser-assisted zona drilling protocols. The Nikon TE300 inverted microscope is used with illumination source and condenser above specimen and objective below. The Petrie dish specimen chamber (wall thickness 1 mm, diameter 50 mm) is on a motorized stage. The eggs settle at the bottom of the dish, and the objective is focused on the edge of the ZP, about 75 μm into the medium.

A typical zona drilling is shown in Figure 1 for a bovine oocyte. The egg diameter is ~150 μm and the thickness of the zona pellucida, the translucent shell surrounding the egg, is ~12 μm. The laser power was set to 100 mW delivered at the focal point, and the three holes depicted in Fig. 1 correspond to pulse duration 1.5, 3, and 4.5 ms. Beam diameter to $1/e^2$ was 6.2 μm, independent of beam power. The hole diameters are 4.3, 7.8, and 10.5 μm; the hole diameter depends more on pulse duration than on laser beam size.

In Figure 2(a) an electron photomicrograph of several channels in a bovine egg is shown. Repeated firing at constant

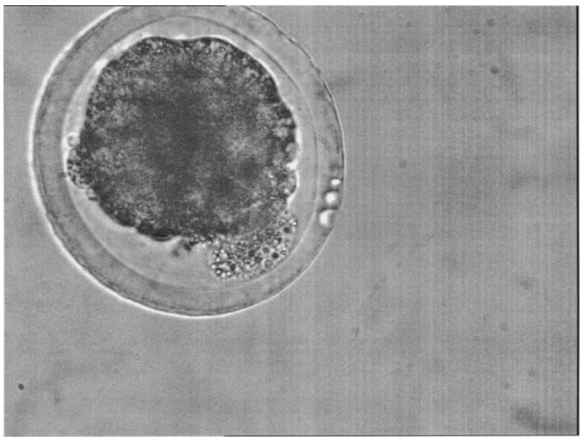

Fig. 1 Laser ablation of ZP of bovine egg at 100 mW, pulse duration 1.5, 3, 4.5 ms.

laser pulse length 25 ms and laser power 50 mW produced channels of consistent size.

The close-up in Figure 2(b) emphasizes the sharply drilled wall of each channel. The channels have clear cylindrical cross sections of width ~12 μm, with no significant beam broadening at either end. The channels reflect a thermal dissolution ''melting'' temperature, and its locus is not coterminous with the beam edge. Although no evidence of thermal damage can be seen surrounding the target area, the transient thermal excursion may cause damage invisible under the microscope to nearby living cells. The thermal history will be derived in the next section.

3 Thermal Predictions

3.1 Standard Conditions

The objective (NA = 0.6, 40×, infinity corrected) used transmits 71% of the incident energy at $\lambda = 1480$ nm. We will take the typical laser beam power arriving at the vicinity of the ZP, following transmissive, reflective, and attenuation loss, as 100 mW. We take the typical beam focal radius as $a = 3$ μm, and assume the beam is passing up through an inverted microscope into medium of refractive index $n = 1.333$. The thermal history expected along the path of the laser beam, and especially in the vicinity of the pre-embryo, will be derived.

3.2 Thermal Constants and Source Function Geometry

The medium is almost pure water, and the cellular material is ~80% water. While the infrared absorptances in the medium and cell at $\lambda = 1480$ nm have not been measured, they are unlikely to be significantly above that of H_2O, and cannot be significantly lower. Similarly, the thermal conductivity of the material will not be higher than that of water. By taking the absorptance as identical to that of H_2O, $\alpha = 21\ \mathrm{cm}^{-1}$ (Ref. 7) we will obtain a lower limit to the temperature produced. On the time scales of interest (1–25 ms), the only significant mode of heat loss from the heated liquid will be thermal conduction, since convection does not have time to develop and radiation may be neglected. The thermal conductivity of water is 6×10^{-3} w/cm/° at room temperature, but since the thermal excursion during the laser pulse is typically 100–200°C, we take the conductivity of the medium as $K = 6.8 \times 10^{-3}$, corresponding to H_2O at 100°C.[16]

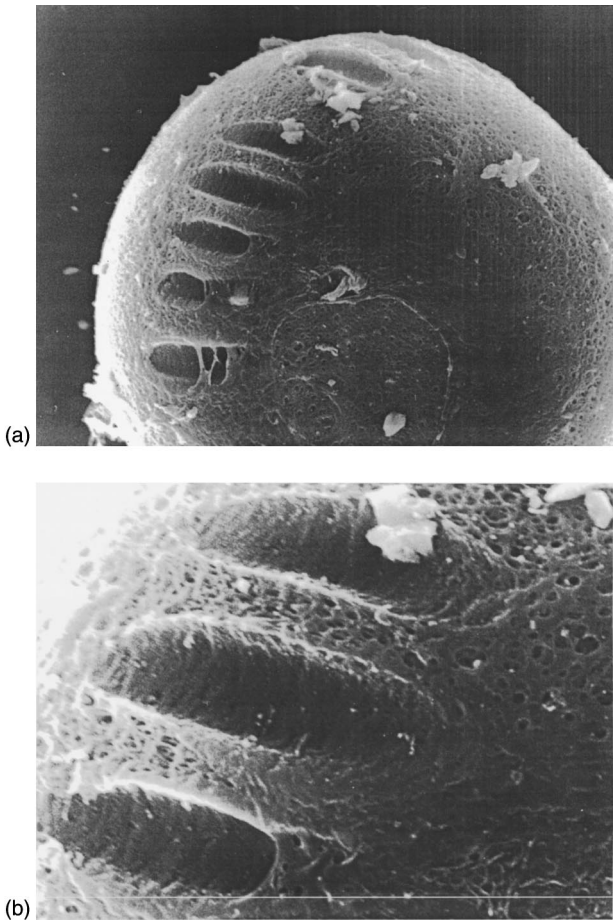

Fig. 2 (a) Bovine egg in which several channels have been cut by laser. (b) Close-up view of channels in bovine zona pellucida. The channels are ~25 μm long, almost constant-radius cylindrical intercepts with sharp edges and do not show effects of beam convergence or divergence.

The laser path is approximated as three regions: (1) a converging cone of semiangle θ, (2) the waist region of the beam, and (3) a diverging cone with semiangle θ. The beam has higher net power at the converging than at the diverging cone, due to attenuation. The cone semiangle is $\theta = \arcsin(\mathrm{NA}/n) = 26.7°$. For the thermal calculation we approximate the waist region as a cylinder of radius $a = 3$ μm and length $2a \cdot \cot\theta$.

The laser beam converges through the medium to a focal point 75 μm above the floor of the Petrie dish. Absorption will only be important in the medium and may be neglected in the Petrie dish. Self-focusing of the IR beam will not significantly affect the thermal distribution outside the beam and is ignored. The radiation intensity is symmetric in azimuthal coordinate, varying in intensity only with axial distance and radius. Ignoring angular variation, the heat diffusion equation in axisymmetric cylindrical coordinates may be written

$$\frac{\partial T}{\partial t} = k\frac{\partial^2 T}{\partial r^2} + k\frac{1}{r}\frac{\partial T}{\partial r} + k\frac{\partial^2 T}{\partial z^2} + \frac{S}{\rho C_p}, \qquad (1)$$

where the heat diffusion coefficient is $k=K/\rho C_p$, and $\rho C_p = 4.18\,\mathrm{j/cm^3}$, so $k=1.6\times10^{-3}\,\mathrm{cm^2/s}$. Variation of the diffusion coefficient with temperature is small and will be ignored. The origin is taken as the focal point, with r and z as the radial and axial distances. The source function S represents the laser heating power per unit volume, and varies across the entire domain.

The source functions in the three regions of the laser path are normalized to the laser power P reaching the focal plane, so that the converging beam is more intense below the waist and attenuates as it progresses upward, diverging above the waist. The central cylinder length is short ($2a.\cot\theta = 12\,\mu\mathrm{m}$), and attenuation is ignored in region 2.

The source functions for attenuated uniform beam in the three regions are

1. Converging

$$S_1=\frac{\alpha P}{2\pi(1-\cos\theta)}\cdot\frac{1}{r^2+z^2}\cdot e^{\alpha(z^2+r^2)^{1/2}}, \tag{2}$$

2. Waist

$$S_2=\frac{\alpha P}{\pi a^2}, \tag{3}$$

3. Diverging

$$S_3=\frac{\alpha P}{2\pi(1-\cos\theta)}\cdot\frac{1}{r^2+z^2}\cdot e^{-\alpha(z^2+r^2)^{1/2}}. \tag{4}$$

The Gaussian profile is approximated by applying the factor $Ae^{-2((\arctan r/z)/\theta)^2}$ to S_1 and S_3, where A is a normalization constant, and for S_2, we use the factor $Ae^{-2(r/a)^2}$.

3.3 Boundaries for Solution of the Heat Diffusion Equation

Equation (1) was solved by finite element analysis (FEA), using the codes COSMOS (Structural Research Co, Los Angeles, CA) and Mathlab PDE Toolbox (Mathworks Inc, Natick, MA), with source functions from Eqs. (2)–(4). The beam travels parallel to the axis of a cylinder of radius 100 μm and length 200 μm. For short pulses ($\tau<6$ ms) these dimensions are sufficient to make edge effects negligible, since the thermal diffusion distance in time τ is $x<30\,\mu$m. The axis is a Neumann boundary with zero radial temperature gradient. Since the beam is attenuated we cannot take the focal plane as a Neumann boundary but have to solve the equation in the entire upper half plane. The cylinder end planes at $z=\pm100\,\mu$m, and cylinder wall at $r=100\,\mu$m, are both Dirichlet boundaries with temperature held at $T_0=37$°C. The initial temperature of the entire domain is taken as T_0.

Of practical interest is the thermal history on the focal plane itself, at various radial distances from the axis, which will give information on the thermal excursion experienced by the nearest blastomeres.

3.4 Preliminary Verification

For comparison with an analytic case, the FEA was run with a uniformly heated cylinder of radius 3 μm in a 200-μm-diam right cylinder containing H_2O at $T_0=37$, and with source function as in Eq. (2), $P=100$ mW and $\alpha=21\,\mathrm{cm^{-1}}$.

The analytic steady-state solution for the temperature difference between edge and center of an infinite cylindrical region of radius $R_{\max}$ heated on axis by a uniform beam of radius R is

$$\Delta T=\frac{\alpha P}{4\pi K}\left[1+2\ln\left(\frac{R_{\max}}{R}\right)\right]. \tag{5}$$

The FEA steady-state result was within 0.5% of the temperature difference from Eq. (5) and we conclude that the system is integrating correctly.

3.5 Standard Case

We take initial temperature in the medium at the physiological $T_0=37$°C, in a cylinder of diameter 200 μm and length 200 μm, with attenuated converging beam of NA=0.6. The field is divided into 1.13×10^5 elements. The same temperature T_0 is held at the end planes and at the radius $R_{\max}=100\,\mu$m. Beam power is 100 mW at the focal waist, with pulse duration 3 ms and radius 3 μm. The problem is solved in the half plane and has been converted to the full plane in Figures 3(a) and 3(b), where the beam direction is bottom to top, shown for times 0.1 and 3 ms, respectively. At 0.1 ms the central temperature is 98.8°C. In Figure 3(b), at 3 ms the central temperature is 189°C. If the beam is flattop instead of Gaussian, central temperature is reduced ~15%. In either case these high temperatures imply the potential presence of superheated medium. The temperature change from the initial value at any time depends on the pulse duration and is directly proportional to the beam power [see Eqs. (1)–(5)]. Predictions for any beam power may be scaled from the results reported.

The effect of attenuation is apparent in the slightly nonvertical slope of the isotherms as the beam progresses from below to above the waist in Figures 3(a) and 3(b). Apart from this effect the converging and diverging parts of the beam away from the end planes result in almost cylindrical isotherms. For the present purpose the focal plane is the only region of interest in questions of cell heating, and we therefore examine whether the focal plane temperature heating can be approximated by a simpler (and faster) one-dimensional solution.

To test the effect of geometry the FEA system was run for the Gaussian beam in the following three cases, all with power 100 mW, pulse 3 ms and radius 3 μm:

1. Attenuated beam, NA=0.6 (converging cone, central cylinder radius 3 μm, converging/diverging cone);
2. Unattenuated beam, NA=0.6 (same as above, exponential terms in Eqs. (2) and (4) set to unity) and
3. Unattenuated beam, NA=0 (uniform central cylinder radius 3 μm, exp. terms set to unity).

The latter case corresponds to a constant cylindrical beam and has one-dimensional symmetry, whereas the first two require two dimensions.

For all three cases, predicted temperatures on the focal plane for radii $5\leqslant\text{radius}\leqslant50\,\mu$m as function of time are

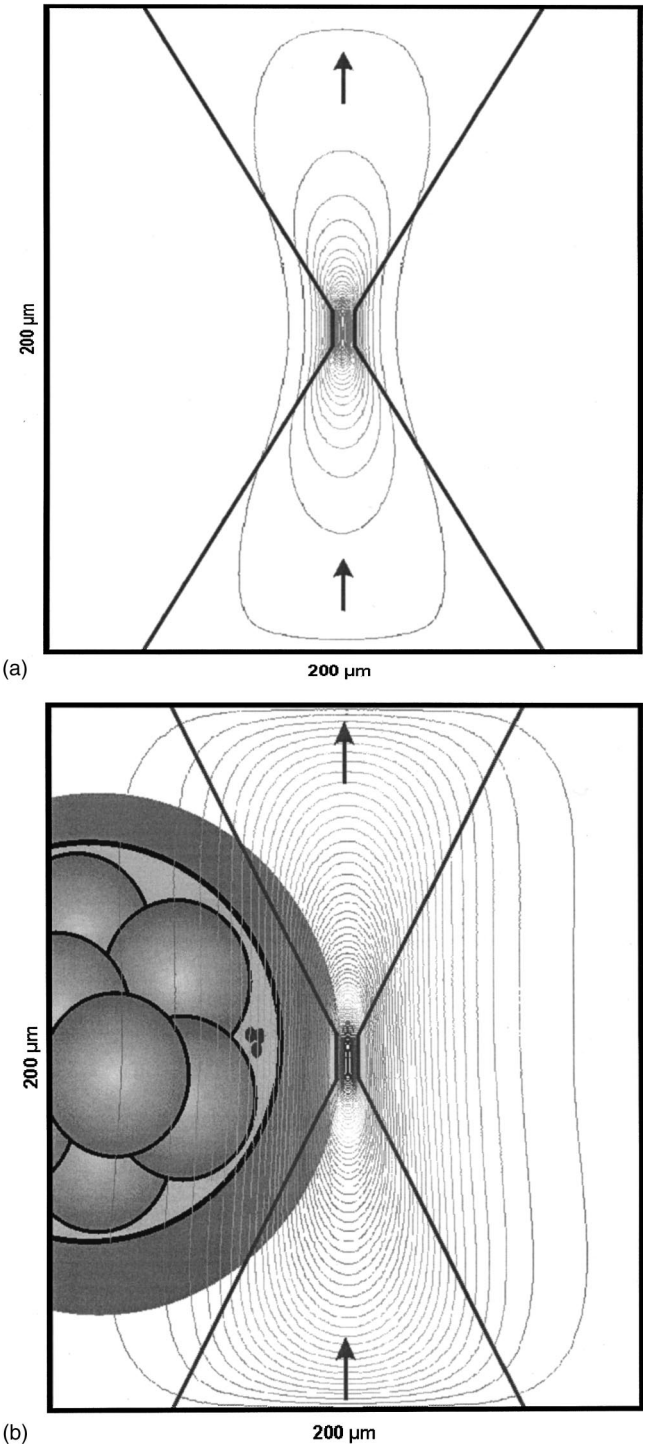

Fig. 3 (a) FEA analysis of 3 ms pulse, 100 mW, converging Gaussian attenuated beam solved in half plane. The isotherms at 0.1 ms into the pulse are indicated. Isotherm interval is 2.5°C. Central temperature is 98.8°C. (b) FEA analysis of same case as 5a, at 3 ms. Isotherm interval is 2.5°C. Central temperature is 189°C.

within 0.5°C over 10 ms integration time. At least on the focal plane, in the present case the converging and diverging beam produces heating very similar to that from a long heated cylinder, and if the power is normalized to its value at the focal plane the effect of beam attenuation may be ignored. Hence the mathematically simpler case of the cylinder can be used for predicting the temperature history at points on the focal plane. In the following we have therefore used the one-dimensional Gaussian elimination solution outlined below.

4 Solution in Cylindrical Symmetry

4.1 Gaussian Elimination

The FEA solution shows that radial temperature history is almost cylindrical, with isotherms close to parallel to the axis over the region of interest. If the heating effect of the beam is approximated as a cylindrical region of constant radius a equal to its focal radius, Eq. (1) can be written as a one-dimensional difference equation, which can be rapidly solved by Gaussian elimination,[17,18] to give the thermal time history in the region near the laser focus. The advantage of this is that solution is much faster than FEA, and the case of pure cylindrical geometry without converging and diverging beams gives a good approximation to the focal plane temperature. We have written a Gaussian elimination (GE) code to model the thermal behavior in the radial dimension.

We cover the area $0 \leqslant r \leqslant R_{\max}$, and take $R_{\max} = 100\ \mu$m, chosen because at the laser pulse lengths considered, the thermal excursion does not reach $R_{\max}$ before the end of the pulse. We divide the cylindrical area into N shells, each separated by $\Delta r = R_{\max}/N$. Accurate results are obtained with $\Delta r = 1\ \mu$m. As boundary conditions, the initial temperature and the temperature at $r = R_{\max}$, are set to $T_0 = 37$°C. The temperature gradient at beam center is set to zero. In the GE analysis we will conservatively assume the beam is flattop rather than Gaussian: this reduces central temperature by ~15% but does not affect temperature history outside the beam. We use Eq. (5) to check the result and find agreement within 0.1% between the GE code and Eq. (5) for very long (200 ms) pulses, so the GE code gives correct results for the analytic case.

4.2 Thermal Histories on Focal Plane

The GE solutions for temperature at various radial positions on the focal plane are shown as function of time in Figure 4. The standard case of beam power 100 mW, pulse duration 3 ms, in a 200 μm right cylinder initially at 37°C is used. At beam center the peak temperature reaches over 170°C. Temperature falls off sharply as the pulse terminates due to the short diffusion time over 3 μm. As expected the thermal excursion seen near the beam has approximately the same duration as the laser pulse.

4.3 Superheating

The calculated (GE) peak central temperatures at typical beam powers with beam radius 3 μm in water are given for flattop beam focal spots of various pulse durations in Table 1, with steady-state values from Eq. (5) for reference. Again we take the region of the analysis as a cylinder of length 200 μm and radius 100 μm. The calculated temperature of water exposed to the beam is very high, with peak central beam temperature ranges up to above 200°C, corresponding to highly superheated water. The question is whether this temperature is real or whether a phase change occurs, which would reduce the central temperature and form a column of vapor bubbles along the beam axis near the focal point. Miotello and Kelly[19] have examined the formation rate of homogeneous nuclei and

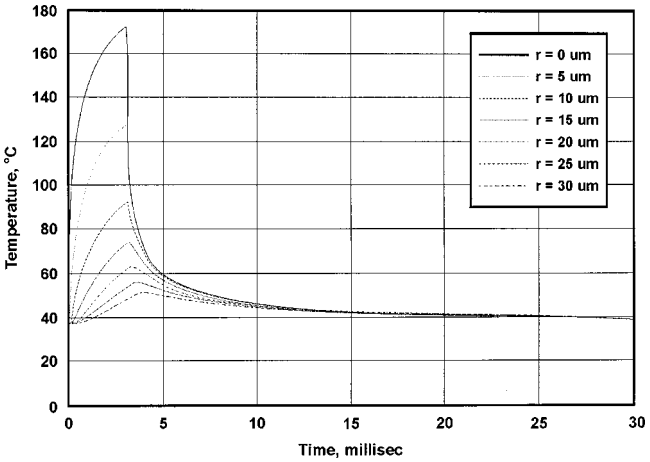

Fig. 4 GE analysis of flattop standard case (100 mW, 3 ms, $a = 3\ \mu$m), beam on axis of a 200 μm right cylinder. Temperature given at various radial distances on focal plane. Using a Gaussian-profile beam increases the central temperature peak by ~15°C, but has a negligible effect on the temperature exterior to the beam.

subsequent explosive phase change in superheated liquids. In the absence of a surface for heterogeneous nucleation, homogeneous nucleation is necessary for rapid phase change, and its rate depends strongly on how close the liquid is to the critical temperature ($T_c = 647$ K for H_2O). The homogeneous nucleation rate becomes significant near 300°C. However, at and below 250°C the rate of homogeneous nuclei formation in water is negligible, and in the absence of sites for heterogeneous nucleation we would not expect boiling within a 25 ms pulse. If nucleation sites are present in the liquid, remote from the walls, boiling could occur. While it is possible that the ZP or local suspended particles may provide sites for nucleation, it is unlikely since sharp solid edges are generally more favorable.

Thermal calculations indicate that highly superheated water is briefly formed in the focal waist of the IR beam. Heat is conducted mainly radially away from the waist, and regions near the beam will be heated by conduction. Superheated water is an excellent solvent, and it is not surprising that the region of ZP within the focal waist rapidly disappears.

After the beam is turned off any vapor bubbles formed would be expected to collapse in less than 1 ms, releasing heat to the liquid. If a significant degree of phase change had occurred the temperature at the beam core would be held to close to 100°C, which would result in lower radial temperatures in the focal plane. We could therefore test the presence of superheating by measuring local temperature excursions.

Table 1 Peak central temperatures.

Power mW	Pulse duration ms	At end pulse °C	Steady state °C
100	1.5	155.4	233.9
100	3.0	172.3	233.9
100	4.5	182.3	233.9
100	6	189.3	233.9
100	10	201.9	233.9
100	15.0	211.7	233.9
100	25	223.0	233.9
80	15.0	176.8	194.5
40	15.0	106.9	115.8

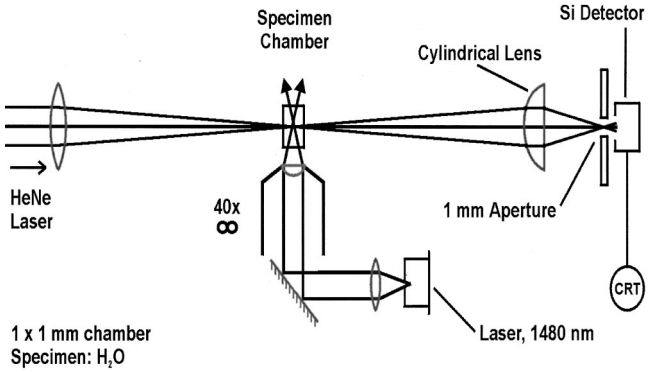

Fig. 5 Measurement of beam steering. Horizontal view.

5 Temperature Check From Probe Beam Steering

5.1 Beam Steering

In order to confirm the predicted temperature excursion, we decided to estimate the change in local refractive index around the IR focal waist caused by the temperature excursion. We used the steering effect caused by the thermal-induced refractive index gradient on an orthogonal probe beam. Estimates show that a 2° change in ray direction would be possible for light passing near the IR heated water column.

5.2 Optical System

The setup is shown in Figure 5. The IR beam passes vertically into a 1×1 mm glass-walled rectangular tube (Vitrocom, Mountain View, NJ) containing distilled H_2O. The laser is set to pulse at 4 Hz, while beam power and pulse duration are varied. The IR beam focus is set at approximately 200 μm above the bottom wall of the rectangular tube. The IR beam focal diameter has already been measured at close to $2a = 6\ \mu$m. A horizontal probe continuous wave (cw) HeNe laser beam is focused with an $f = 120$ mm lens into the region of the IR beam focus, with the HeNe optic axis orthogonal to the IR beam axis. The HeNe probe beam radius to the $1/e^2$ points at its focal point was measured by knife intercept as $22.3 \pm 1.2\ \mu$m. The probe covers the region of interest near the IR focus. The HeNe beam is then focused with a cylindrical lens on to a 1 mm aperture in front of a Si detector. By scanning the aperture+detector in the direction orthogonal to both laser axes, the angle by which the probe beam is refracted (or scattered) by the thermal field around the IR beam is determined. The system is used to measure the maximum

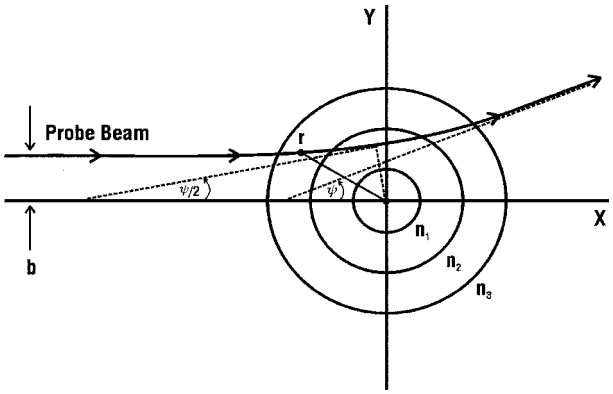

Fig. 6 Bending of ray with impact factor b near a central refractive field. Vertical view.

angle through which the probe beam is turned at given pulse length/power. This is then compared with the angle derived from the predicted thermal field.

5.3 Probe Ray Steering

The curvature of the probe ray is proportional to (and in the direction of) the normalized refractive index gradient $\nabla n/n$. In the IR beam focal plane the temperature field, and consequently the refractive index, in the specimen must be radially symmetric around the IR axis. The refractive index will decrease toward the IR axis during the IR pulse, and a probe ray traveling in the focal plane of the IR beam will be steered away from the axis (see Figure 6). The steering angle Ψ in a centrally symmetric refractive field[20] is given by the expression

$$\Psi = \pi - 2 \cdot \int_R^\infty \left[r \sqrt{\left(\frac{nr}{b}\right)^2 - 1} \right]^{-1} \cdot dr, \qquad (6)$$

where b is the impact factor, r is radial distance from the IR beam axis, $n(r)$ is the refractive index, and $R = b/n(R)$ is the distance of closest approach.

The refractive index $n(T)$ of superheated water is given by IAPWS[21] from 0 to 150°C. This covers the required range except for the beam center. For higher temperatures we have extrapolated from the IAPWS data. We use the GE solutions for the thermal field to calculate $n(r)$, and derive the expected probe ray steering by the changed refractive index during the laser pulse, as a function of IR laser power and pulse length. The impact factor covers the range $0 < b < 22\ \mu$m due to the large probe beam diameter.

The maximum beam bending is a measure of the maximum temperature gradient, which occurs adjacent to the beam radius and corresponds to the specific temperature field. The predicted values for pulse duration 25 and 2.5 ms are shown, and maximum measured steering angles are given in Figure 7 for IR power 20–100 mW and pulse duration 1–25 ms. The laser power shown in Figure 7 is that delivered at the focal point, allowing for absorption after 200 μm H_2O.

After the beam is turned off any vapor bubbles formed would be expected to collapse in less than 1 ms, releasing heat to the liquid. We will neglect possible phase change in the

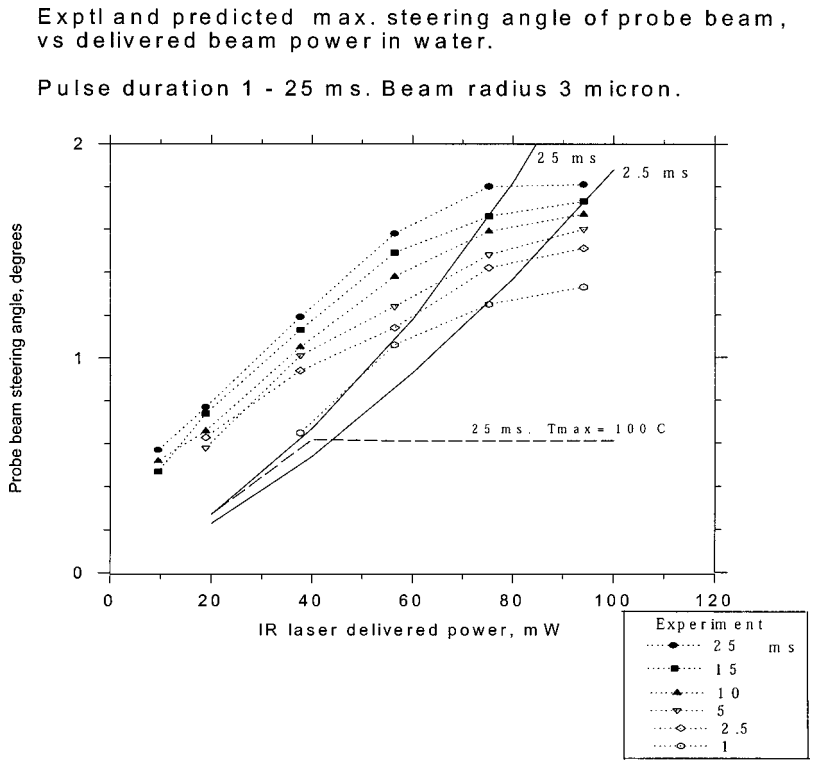

Fig. 7 Probe beam steering angle in the IR laser thermal field, vs delivered IR power. Measurements are denoted by symbols and predictions by solid lines. The dashed line corresponds to the prediction when maximum temperature cannot exceed 100°C.

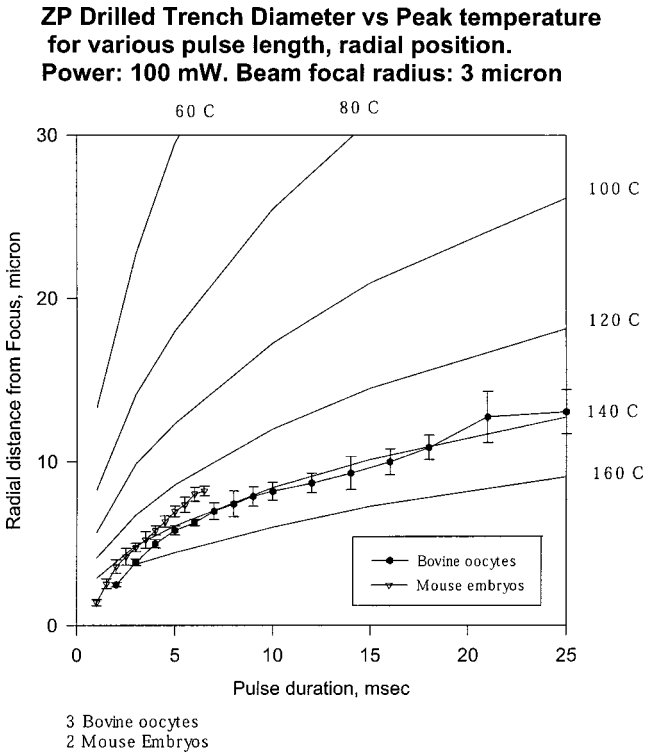

Fig. 8 Measured channel diameter vs pulse duration averaged over three bovine eggs and two murine embryos. Predicted maximum temperature in focal plane at given radius is shown vs pulse duration and radial distance from axis.

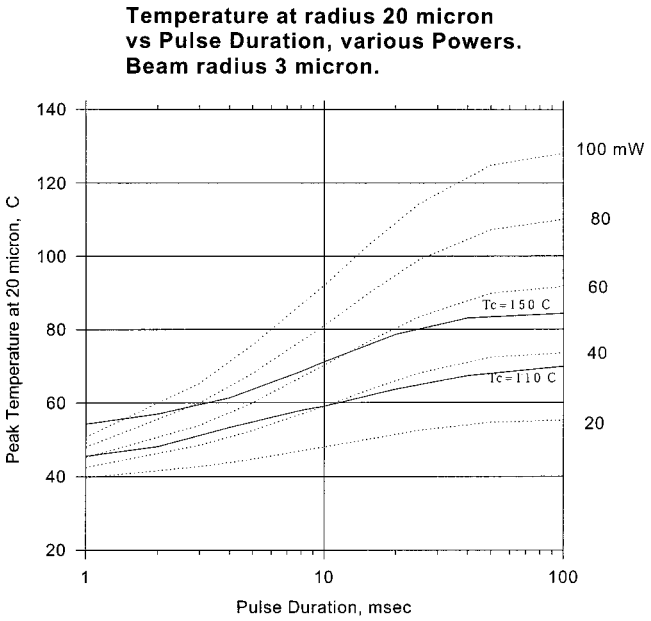

Fig. 9 The predicted maximum of the temperature pulse 20 μm from beam axis in the focal plane is given vs laser pulse duration and beam power. Also shown are limit lines corresponding to beam central temperature 150 and 110°C.

time scales of interest. Consequently, we can use predictions derived from Eq. (1) to compute temperatures in the beam focal plane.

For higher laser delivered power, the central temperature rises and the thermal gradient becomes steeper. The predicted values therefore increase. The measured values show a tendency to reach a limiting value at high laser powers, in the region where the predicted temperature is >200°C, implying that the gradient has maximized. This is unlikely to reflect phase transition: once phase change nucleates at these superheated temperatures, it would be expected to continue until the medium reaches $T=100$.

We note that, if the medium can reach a maximum temperature of only 100°C due to phase change, the predicted refractive index gradient never rises high enough to cause the observed beam bending, but flattens out at $\theta=0.6°$. Since the observed maximum ray bending angle is $\theta=1.8°$, the results are consistent with central beam temperature >100°C.

5.4 "Melting Point" of Zona Pellucida

We have measured the diameter of the channels cut in the ZP of three bovine oocytes by pulses of power 100 mW and duration 1.5–25 ms, using a 3 μm radius beam under standard conditions. We have also measured channels cut in the ZP of murine two-cell pre-embryos by the same beam. The channel diameter versus pulse duration is shown for both species in Figure 8. The GE model is applied to determine temperature history on the focal plane at various distances from the beam axis, and the peak temperature calculated at each position is shown in Figure 8.

The bovine ZP material appears to undergo dissolution (melt) between 140 and 150°C, the temperature decreasing with longer pulse time. The murine ZP appears to be more easily removed and vanishes at ~5–10°C lower temperature than the bovine.

Descloux and Delacrétaz[22] measured the thermal dissolution of mouse ZP at temperatures 61–73°C over times up to 1000 s, and derived a rate constant. We extrapolate this to estimate the mouse ZP dissolution temperature for 10 ms pulse as 111°C, lower than our experimental estimate averaged over the ZP from mouse pre-embryos. The minimum temperature that must be attained in the beam center in order to ablate human ZP material in the pulse times used is likely to be between 130 and 150°C.

6 Conditions for Minimizing Collateral Damage

Conservatively, we will assume that the beam central temperature should be maintained at or above ~150°C in order to penetrate the ZP within pulse time of 10 ms. At the same time the temperature at the surface of the nearest cell should be minimized. We take typical distance to nearest cell as 20 μm, and use the thermal model above to derive temperatures on the focal plane at 20 μm from the beam axis: in Figure 9 a graph is shown of the peak temperature reached during the pulse as function of pulse duration, for various beam powers. In the present case a typical thermal excursion would last on the order of the pulse duration, and have peak amplitude shown. The cells therefore undergo rapid heating and cooling of amplitude tens of degrees in a few milliseconds.

We are not aware of published work on the deleterious effects of brief thermal pulses on cells. If we assume thermal

damage scales as a chemical reaction, then damage would be proportional to $\tau \cdot \exp(-\Delta Q/RT)$, where τ is pulse duration, T is the mean pulse temperature, and ΔQ is reaction energy. This would imply that the pulse time must be kept extremely short if the temperature rise is significant.

It is clearly advisable to minimize the thermal excursion amplitude and duration, both of which imply keeping pulse time low. Short pulse duration and high beam power give the most efficient system for maximizing beam cutting power and minimizing local heating. We have indicated in Figure 9 limiting lines corresponding to beam center peak temperatures of 150 and 110°C. The peak central temperature should exceed the limiting lines for rapid ZP ablation, while maintaining minimum peak temperature at 20 μm. It is evident that the laser pulse duration should be as short as possible consistent with effective ZP dissolution, preferably below 5 ms.

7 Summary and Conclusion

IR laser beams introduced into the optical path of an inverted microscope are now routinely used to perform delicate operations on human pre-embryos *in vivo*. The ablative properties of a pulsed beam of $\lambda = 1480$ nm laser light are of considerable interest for penetration of the shell surrounding the pre-embryo. Using the laser, highly predictable and reproducible results are obtained and the amount of time necessary to perform a treatment on pre-embryos is kept very short. The introduction of laser technology into the clinical IVF laboratory has allowed the development of more standardized procedures which are not so dependent on individual operator skill.

The action of the laser must be strictly limited to the targeted region of the ZP, since focused laser irradiation on any cell would be damaging and probably fatal to that cell. Following irradiation the heat is conducted away from the target onto which the laser focal spot is directed, and is dissipated into the surrounding medium. Our interest is to determine the temperature in the medium exposed to the beam and its surroundings, and set limits to beam pulse and beam power. We have examined the thermal regime associated with pulsed laser ablation of pre-embryo zona pellucida, and found that a one-dimensional model gives adequate accuracy to predict temperature. Only conductive heat transfer is important, and the result that the aqueous medium in fact reaches superheated temperatures in the laser beam is obtained. Experiment confirms the presence of the high thermal gradients predicted in the medium. We estimate the temperature of zona pellucida ablation in bovine oocytes between 140 and 160°C, and murine embryos 130–150°C. Potentially damaging thermal excursions at the embryo blastomeres are minimized by using pulse durations 1–5 ms.

References

1. J. Cohen, M. Alikani, J. Trowbridge, and Z. Rosenwaks, ''Implantation enhancement by selective assisted hatching using zona drilling of human embryos with poor prognosis,'' *Hum. Reprod.* **7**, 685–691 (1992).
2. W. B. Schoolcraft, T. Schlenker, G. S. Jones, and H. W. Jones, ''*In vitro* fertilization in women age 40 and older: The impact of assisted hatching,'' *J. Assist Reprod. Genet.* **12**, 581–584 (1995).
3. M. Germons, D. Nocera, A. Senn, K. Rink, G. Delacrétaz, Pedrazzini, and J. P. Hornung, ''Improved fertilization and implantation rates after non-touch zona pellucida microdrilling of mouse oocytes with a 1.48 μm diode laser beam,'' *Hum. Reprod.* **11**, 1043–1048 (1996).
4. L. Gianaroli, M. C. Magli, A. P. Ferraretti, A. Fiorentino, J. Garrisi, and S. Munné, ''Preimplantation genetic diagnosis increases the implantation rate in human *in vitro* fertilization by avoiding the transfer of chromosomally abnormal embryos,'' *Fertil. Steril.* **68**, 1128–1131 (1997).
5. M. Montag, K. van der Ven, G. Delacrétaz, K. Rink, and H. van der Ven, ''Laser-assisted microdissection of the zona pellucida facilitates polar body biopsy,'' *Fertil. Steril.* **69**, 539–542 (1998).
6. A. Veiga, M. Sandalinas, M. Benkhalifa, M. Boada, M. Carrera, J. Santalo, P. N. Barri, and Y. Ménézo, ''Laser blastocyst biopsy for preimplantation diagnosis in the human,'' *Zygote* **5**, 351–354 (1997).
7. *Handbook of Optics*, W. G. Driscoll, Ed., Optical Society of America, McGraw–Hill, New York (1978).
8. K. Rink, G. Delacrétaz, R. P. Salathe, A. Senn, D. Nocera, M. Germond, P. de Gamdi, and S. Fakan, ''1.48 μm diode laser microdissection of the zona pellucida of mouse oocytes,'' *Biomedical Optics. International Soc. For Optical Engineering, Proc. SPIE* **2134A-53** (1994).
9. K. Rink, G. Delacrétaz, R. P. Salathe, A. Senn, D. Nocera, M. Germond, P. de Gamdi, and S. Fakan, ''Non contact microdrilling of mouse zona pellucida with an objective-delivered 1.48 μm diode laser,'' *Lasers Surg. Med.* **18**, 52–62 (1996).
10. M. Germons, D. Nocera, A. Senn, K. Rink, G. Delacrétaz, and S. Fakan, ''Microdissection of mouse and human zona pellucida using a 1.48 μm diode laser beam: efficacy and safety of the procedure,'' *Fertil. Steril.* **64**, 604–611 (1995).
11. K. Kanyo, ESHRE Proceedings, Bologna, Italy (2000).
12. M. Germons, D. Nocera, A. Senn, K. Rink, and G. Delacretaz, ''Assisted hatching of frozen-thawed embryos with a 1.48 μm diode laser enhanced pregnancy outcome in patients who had several nidation failures,'' *Abstract of the Annual Meeting of the American Society for Reproductive Medicine*, P-051, S116 (1996).
13. Z. P. Nagy, L. Rienzi, M. Iacobelli, F. Morgia, F. Ubaidi, M. Schimberni, and C. Aragona, ''Laser assisted hatching and removal of degenerated blastomeres of frozen-thawed embryos improves pregnancy rate,'' *Fertil. Steril. 72 (suppl. 1) Abstract of the Annual Meeting of the American Society for Reproductive Medicine*, **O-09**, S4 (1999).
14. Y. Liu, D. K. Cheng, G. J. Sonek, M. W. Berns, C. F. Chapman, and B. J. Tromberg, ''Evidence for localized cell heating induced by infrared optical tweezers,'' *Biophys. J.* **68**, 2137–2144 (1995).
15. P. Cellier and J. Conia, ''Measurement of localized heating in the focus of an optical trap,'' *Appl. Opt.* **39**, 3396–3407 (2000).
16. *Handbook Chem. Phys.*, R. Weast, Ed., CRC, Boca Raton (1984).
17. D. Potter, *Computational Physics*, Wiley, New York (1972).
18. S. Koonin, *Computational Physics*, Benjamin Cummings (1986).
19. A. Miotello and R. Kelly, ''Laser induced phase explosion: New physical problems when a condensed phase approaches the thermodynamic critical temperature,'' *Appl. Phys. A: Mater. Sci. Process.* **69**, S67–S73 (1999).
20. M. Born and E. Wolf, *Principles of Optics*, 6th ed., Pergamon, New York (1980).
21. R. B. Dooley, ''Release on the refractive index of ordinary water substance as a function of wavelength, temperature and pressure,'' *International Association for the Properties of Water and Steam*, EPRI, Palo Alto, CA, 94394 (1977).
22. L. Descloux and G. Delacrétaz, Inst. Appl. Optics DM2-10A EPFL, Lausanne (1999).